Electrical conductivity and microstructure relationship in ternary systems based on cerium oxide

A.L. Horovistiz[1], R.A. Rocha[2], E.N.S. Muccillo*

Energy and Nuclear Research Institute-IPEN, PO Box 11049, S. Paulo, SP 05422-970 Brazil

Abstract

The effects of small amounts of bismuth and sodium on the electrical conductivity of gadolinia-doped ceria are investigated. Bulk specimens of nominally pure $Ce_{0.9}Gd_{0.2}O_{1.9}$ and $Ce_{0.8}Gd_{0.19}M_{0.01}O_{1.9}$ with M=Bi or Na were prepared by the cation complexation technique. Raman spectra of sintered specimens show a prominent band at approximately 464 cm^{-1} assigned to the cubic fluorite-type lattice of cerium oxide. Both additives promoted changes in the microstructure of samples sintered at 1723 K. Bi-containing samples exhibit low porosity along with angular grains with mean grain size of about 1.7 μm compared to 1.4 μm of pure gadolinia-doped ceria. Addition of Na to gadolinia-doped ceria reduced the mean grain size (1.0 μm) but porosity increased drastically. Electrical conductivity measurements were used to study mass transport. Analysis of impedance spectroscopy data shows that the apparent activation energy for conduction is slightly lower in samples containing the additives explaining the higher grain and grain boundary conductivities of the ternary systems.
© 2013 Elsevier Ltd and Techna Group S.r.l. All rights reserved.

Keywords: A. Powders: chemical preparation; C. Ionic conductivity; D. CeO$_2$; E. Fuel cells

1. Introduction

Gadolinia-doped ceria, CGO, is a promising solid electrolyte for application in intermediate-temperature (500–700 °C) solid oxide fuel cells, due to its superior ionic conductivity compared to yttria-stabilized zirconia [1,2]. The high oxide ion conduction behavior of doped cerias is a consequence of partial substitution of cations of lower valence, such as trivalent rare-earths and alkaline-earths, for Ce^{4+}. In these substitutional solid solutions, increasing of the chemical stability and enlargement of the electrolytic domain are observed when compared to undoped cerium oxide [2–4].

Over the last years several investigations have been carried out aiming to improve the electrical performance of ceria-based solid electrolytes by the introduction of a second additive. This approach has allowed to obtain higher grain or grain boundary conductivity, depending on the type and content of the additive [5–8].

Small amounts of a second additive have been used as well to increase the sinterability of ceria-based solid electrolytes. In this case, the additive is expected to provide faster densification kinetics thereby lowering the sintering temperature, as predicted by Herring's scaling law [9]. In this case, transition metal oxides have been extensively studied [10,11]. In general, these additives enhanced the sinterability of gadolinia-doped ceria, mainly those with relatively low melting point.

In some studies the second additive has been chosen randomly. Recently, the concept of cation mismatch minimization along with Vegard's slope have been applied with success [5,12].

Addition of bismuth to gadolinia-doped ceria has been already reported [13–16]. Gil et al. [13] determined the low solubility of Bi in CGO (about 0.76 mol%). The rate of grain growth in co-doped specimens was smaller than in pure CGO, and no significant change in the overall electrolyte conductivity was found. Increased sinterability of the ternary system was

*Corresponding author. Tel.: +55 11 31339203; fax: +55 11 31339276.

   E-mail address: enavarro@usp.br (E.N.S. Muccillo).

[1]Present address: Ceramics Department (CICECO), University of Aveiro, 3810-193 Aveiro, Portugal.

[2]Present address: Federal University of ABC, UFABC, S. Andre, 09090-400, SP, Brazil.

attributed to liquid phase sintering [14] due to bismuth addition. $Ce_{0.8}$ $(Gd_{1-x}Bi_x)_{0.2}O_{1.9}$ ($x=0.1–0.5$) compositions were prepared by the coprecipitation technique by Fu et al. [15]. They also found that the sintering temperature of CGO can be reduced by bismuth addition. Heavier additions of Bi_2O_3 to CGO were investigated by Huang and Li [16]. They found that an ideal concentration of about 25 wt% of Bi_2O_3 to CGO maximized the activity of direct methane oxidation without syngas cogeneration at low temperature. The system was then proposed for application as anode material in solid oxide fuel cells.

In contrast, no reports were found relating addition of sodium to CGO. The effects produced by other alkali ions in CGO are reported in [12], where addition of 3 mol% Li and K to CGO have resulted in different behaviors. The sintering temperature was drastically reduced (to about 1073 K) with Li addition, whereas K inhibited sintering. These contrasting effects were attributed to the quite different Vegard's slope.

Another important question concerning the use of additives during ceramic processing is the degree of dispersion, which is favored by the use of chemical methods [17]. In special, for multicomponent compositions, preparation methods based on gel-, glass- or vitreous-like precursors are preferred to other solution methods, because the diffusion rates are slowed down in these matrices avoiding (or minimizing) the segregation of minor components [18].

In this work, gadolinia-doped ceria pure and containing small amounts of Bi and Na as additives were chemically synthesized by the cation complexation technique. These cations have similar radius in 8-fold coordination ($r_{Bi}=1.17$ Å, $r_{Na}=1.18$ Å [19]). Moreover, bismuth and sodium possess moderate absolute values of Vegard's slope and are expected to produce liquid phase sintering of CGO [12]. The main purpose of this investigation is to verify the effects of these additives on the grain and grain boundary conductivities of gadolinia-doped ceria solid electrolyte prepared from nanosized powders.

2. Experimental

2.1. Sample preparation

Cerium nitrate ($(CeNO_3)_3 \cdot 6H_2O$, 99.99%, Aldrich), gadolinium oxide (Gd_2O_3, 99.9%, Aldrich), and bismuth and sodium carbonates, both of reagent grades, were used as starting materials. Solid solutions with nominal compositions $Ce_{0.8}Gd_{0.2}O_{1.9}$ and $Ce_{0.8}Gd_{0.19}M_{0.01}O_{1.9}$ with M=Bi or Na were prepared by the cation complexation technique according to the procedure described [20]. The samples containing Bi and Na will be denoted as CGO-Bi and CGO-Na, respectively. In this method, the proper amount of each cation nitrate or carbonate was used to prepare a stock solution. The cation solutions were first mixed together in the desired proportion and then added to an aqueous solution of citric acid with a metal/citric acid ratio of 1:2. The resultant clear solution was heated to about 373 K to form a

transparent gel. Continuous stirring and heating of the gel gave rise to a sponge-like resin with homogeneous cation distribution. The precursor resins were first heat treated at 523 K for 1 h to allow for partial elimination of the organic matter. A subsequent calcination was performed at 1073 K for 1 h resulting in white (Na added) or pale yellow (pure and Bi added) nanopowders. Cylindrical pellets were prepared by uniaxial pressing at 20 MPa followed by cold isostatic pressing at 100 MPa and sintering at 1773 K for 3 h in air.

2.2. Characterization

Structural characterization of sintered pellets was carried out by Raman spectroscopy (Renishaw, InVia Raman Microscope) coupled to a Leica optical microscope, with an excitation radiation of 633 nm from a He–Ne laser. Field emission scanning electron microscopy, FE–SEM (FEI, Inspect F50) was used to observe microstructural features in sintered pellets after polishing and thermal etching. The ionic conductivity was determined by electrochemical impedance spectroscopy using a low-frequency impedance analyzer (4192 A Hewlett Packard) in the 5 Hz to 13 MHz and 453–673 K frequency and temperature ranges, respectively. Silver was used as an electrode material.

3. Results and discussion

3.1. Structure and microstructure characterizations

Fig. 1 shows Raman spectra of CGO, CGO-Bi and CGO-Na samples after sintering. In the 200–800 cm^{-1} spectral range all spectra exhibit a prominent Raman band centered at 464 cm^{-1} (CGO) and 463 cm^{-1} (CGO-Bi and CGO-Na) characteristic of the optical F_{2g} triple degenerated mode of the fluorite lattice, which originates from oxygen stretching vibrations. According to McBride et al. [21], this band with strong intensity becomes asymmetric when solid solutions are formed in the cubic ceria lattice giving rise to a long low-frequency tail. This effect is clearly identified in Fig. 1. In
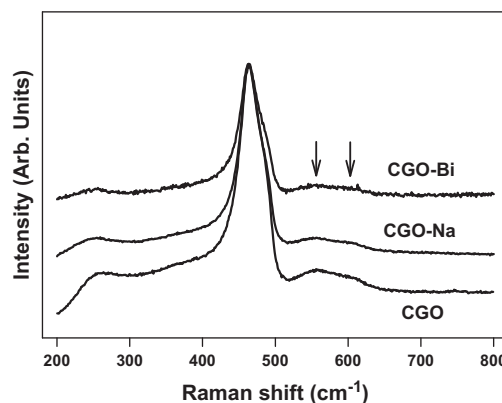

Fig. 1. Raman spectra of CGO, CGO-Bi and CGO-Na sintered pellets. The arrows indicate the Raman bands assigned to the presence of oxygen ion vacancies.

addition, two bands with low intensity indicated by arrows are detected in the 520–640 cm^{-1} range attributed to oxygen vacancies. No difference was detected among the spectrum of pure CGO sample and those of ternary systems due to the small nominal content (1 mol%) of the additives.

Fig. 2 shows scanning electron microscopy micrographs of representative micro-regions of (a) pure $Ce_{0.9}Gd_{0.2}O_{1.9}$ and CGO containing 1 mol% (b) Bi and (c) Na sintered specimens. The main microstructural features of CGO (Fig. 2a) are polygonal grain shape along with a relatively wide distribution of grain sizes. Porosity is mostly confined on the grain boundaries and triple grain junctions. Grain pullout is also observed. The microstructure of CGO-Bi (Fig. 2b) exhibits negligible porosity evidencing the densifying character of this additive. The shape of the grains is predominantly polygonal except for the smallest grains, which tend to be spherical. Some grain boundaries are bended revealing liquid formation during sintering. However, due to the small amount of the additive, the volume fraction of liquid formed at the sintering temperature is expected to be small. Furthermore, similar to CGO, grain size distribution is wide. For CGO-Na samples (Fig. 2c) the grain shape shows a tendency to roundness probably due to a substantial volume of liquid formed during sintering along with possible small solubility of sodium in the

matrix. The grain size distribution is similar to those of CGO and CGO-Bi, and extensive porosity and grain pullout are observed. This latter effect seems to be a result of embrittlement of the grain boundaries due to Na. The mean grain sizes are 1.4 (CGO), 1.7 (CGO-Bi) and 1.0 μm (CGO-Na). A full description of the microstructure features in ternary ceria-based systems by digital image analysis was already reported [22].

3.2. Electrical conductivity

The additives have higher cation radius compared to that of Ce^{4+} ($r_{Ce} = 0.97$ Å [18]) and, thus, a limited solubility is predicted even at high temperatures. Then, it may be expected that bismuth addition to CGO will act on both grain (g) and grain boundary (gb). A similar behavior related to solubility and ionic conductivity is expected for additions of Na to CGO, although no data was found on the solubility of this additive in ceria.

Fig. 3a shows typical impedance spectroscopy diagrams recorded at 568 K. In the temperature range of measurements the impedance diagrams show similar features, i.e., two well-resolved semicircles due to the bulk resistivity (high frequency)
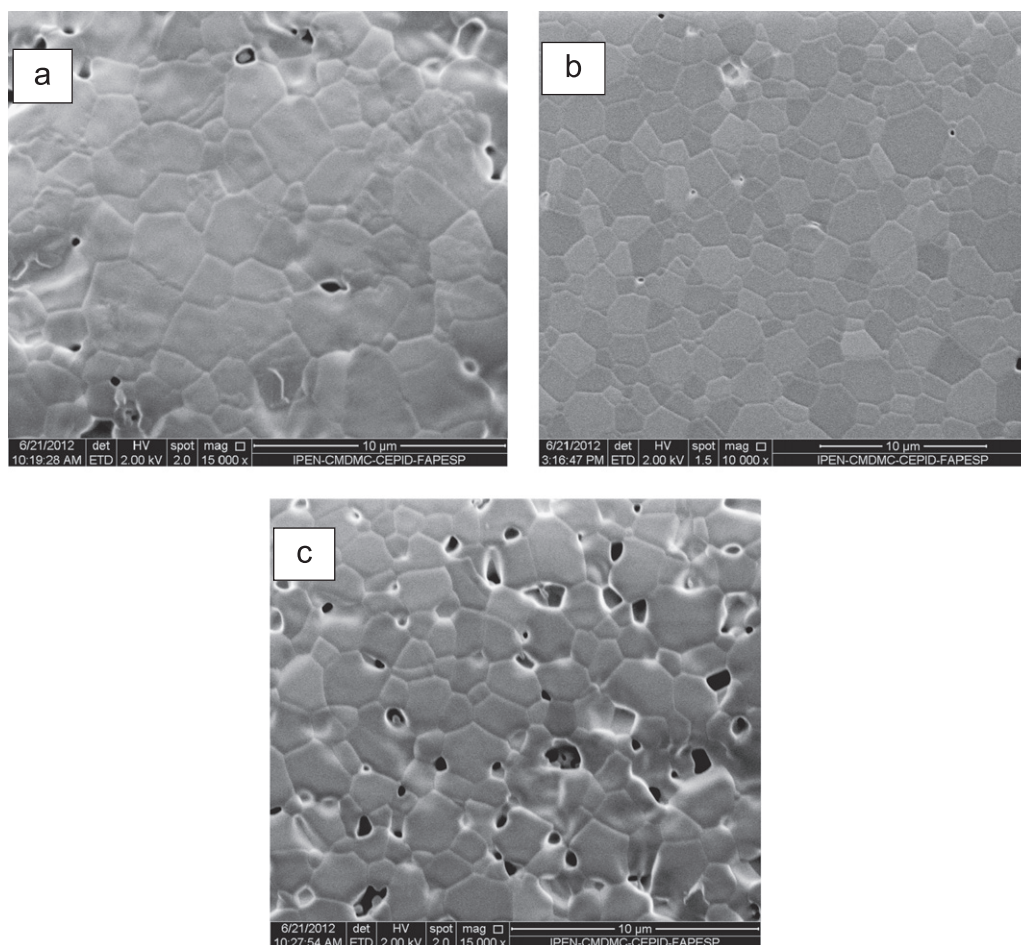

Fig. 2. FE–SEM micrographs of (a) pure $Ce_{0.9}Gd_{0.2}O_{1.9}$ and containing (b) Bi and (c) Na sintered pellets.

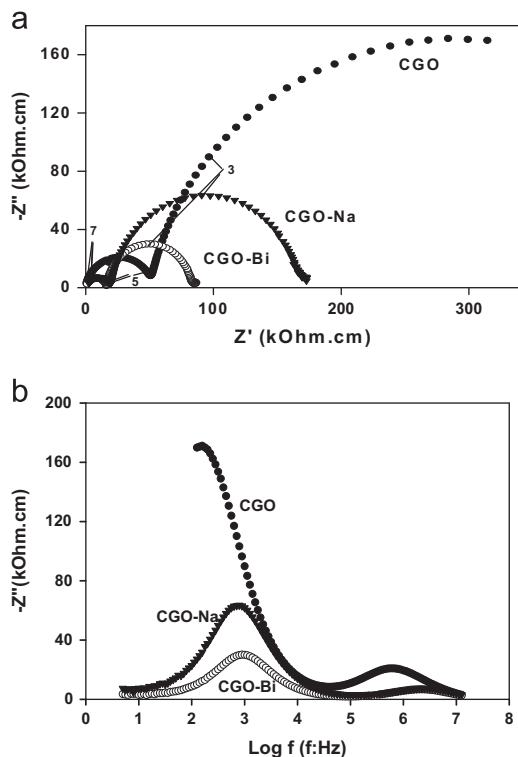Fig. 3. (a) Impedance spectroscopy diagrams and (b) [-Z″ (w) × Log f] plots of pure $Ce_{0.9}Gd_{0.2}O_{1.9}$ and ternary systems at 568 K. Numbers stand for the logarithm of the frequency (Hz).

and to the blocking effect at grain boundaries (low frequency). In these plots, the experimental data of each specimen were normalized for sample dimensions for comparison purposes. It can be seen that specimens containing additives, CGO-Bi and CGO-Na, exhibit lower grain and grain boundary resistivities. This is an indication that both additives are only partially soluble in the CGO lattice, and the excess remains at the grain boundaries. A further indication of the partial incorporation of the additives is the variation of the frequency in the apex (*f*) of each semicircle. This parameter is usually considered as characteristic of a given composition and then, it may be used as a "fingerprint" of the relaxation phenomena [23]. Fig. 3b shows [-Z″ × log f] plots for the studied specimens at the same temperature of 568 K. For samples containing additives, the frequency at maximum amplitude of each peak is shifted to high value in comparison to that of CGO. The shift in the frequencies is quite similar for both additives.

Table 1 lists capacitance, *C*, values for grains and grain boundaries calculated from the frequency in the apex, *f*, of each semicircle and the resistance, *R*, determined by the diameter of the semicircle from: $2 \pi f RC = 1$. The capacitances of all studied compositions are of the same order of magnitude of pF for the high frequency and nF for the low frequency semicircles, as expected. The semicircles center fall below the real axis as in other ionic conductors, and the off-axis angles for grain (φ_g) and grain boundaries (φ_{gb}) are listed in Table 1. Decrease of φ_{gb} reveals that both additives exert a beneficial effect to the homogeneity of the grain boundaries [23].

The Arrhenius plots of the electrical conductivity of grains (a) and grain boundaries (b) are shown in Fig. 4. The grain conductivity (Fig. 4a) is higher for CGO-Na than for CGO specimens. The grain conductivity of CGO-Bi is slightly lower than that of CGO-Na. This result evidences that both additives contribute to improve the grain conductivity of CGO. Maximization of the grain conductivity may be obtained either by increasing the fraction of oxygen vacancies available for conduction or by reducing the energy barrier for oxygen vacancy migration. The grain boundary conductivity (Fig. 4b) is higher for samples containing bismuth and sodium compared to CGO. In this case, the grain boundary conductivity of specimens containing additives is not as close as the grain conductivity meaning that the additives act differently at the intergranular regions.

Activation energy values for grain and grain boundary conductivity obtained by fitting of experimental data are listed in Table 1. These values were obtained from the frequency plots (Log f × 1000/T) not shown here, which do not dependent on sample dimensions and thus, the error in the activation energy values is minimized (± 0.02 eV). The activation energy for grain and grain boundary conduction is lower in specimens containing additives demonstrating the improved conducting properties of ternary systems.

The effect of the additives on the grain boundary conductivity can, in a first instance, be analyzed in terms of the grain boundary area. As the addition of bismuth and sodium to gadolinia-doped ceria modify the grain boundary area, Fig. 5 shows the temperature dependence of the grain boundary conductivity normalized for the mean grain size.

At a fixed temperature, the normalized grain boundary conductivity of CGO-Bi is nearly one order of magnitude higher than that of CGO. In addition, the activation energy for grain boundary conduction (Table 1) is lower in CGO-Bi. Therefore, in the restricted temperature range of measurements, the improvement of the grain boundary conductivity in CGO-Bi might be explained as a result of increased mass transport along the grain boundaries. Particularly, for CGO-Na specimens the effects of the additive were to reduce the mean grain size (or increasing the grain boundary area) and act as a pore former (Fig. 2c). Both effects are known to increase the blocking of charge carriers at the grain boundaries. In order to compare the blocking effect in the studied compositions, the blocking factor (α_R) was evaluated from [23]: $\alpha_R = R_{gb}/R_T$, where R_T is the sum of the grain (R_g) and the grain boundary (R_{gb}) resistances. Fig. 6 depicts the temperature dependence of α_R.

The tendency to decrease the blocking factor with increasing temperature may be seen for all studied specimens. At any temperature the blocking effect at grain boundaries is lower for CGO-Bi compared to CGO. This means that small additions of bismuth are efficient to increase the mass transport along the grain boundaries of gadolinia-doped ceria, even taking into account its partial solubility in the matrix. In the case of CGO-Na, α_R is also lower than that in CGO.

Table 1
Values of capacitance, C, off-axis angle, φ, and activation energy, E, for grain (g) and grain boundary (gb).

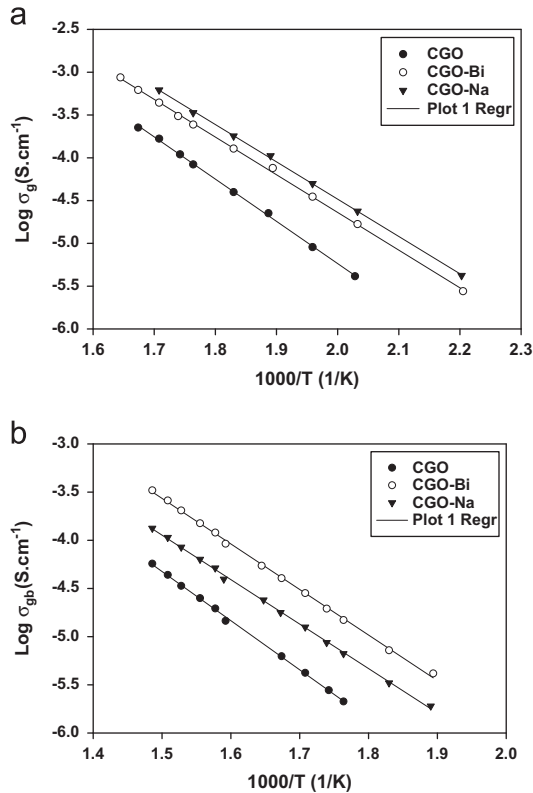| Specimen	C_g [a] (pF cm^{-1})	φ_g [b] (deg.)	C_{gb} [a] (nF cm^{-1})	φ_{gb} [b] (deg.)	E_g [c] (eV)	E_{gb} [c] (eV)
CGO	4.7	14.5	1.8	15.0	0.98	1.07
CGO-Bi	9.4	11.7	2.5	6.5	0.86	0.94
CGO-Na	8.6	14.5	3.5	9.8	0.85	0.93

[a] values determined at 568 K.
[b] average value.
[c] determined from fitting of the frequency plots.

Fig. 4. The Arrhenius plots of (a) grain and (b) grain boundary conductivities of CGO, CGO-Bi and CGO-Na.
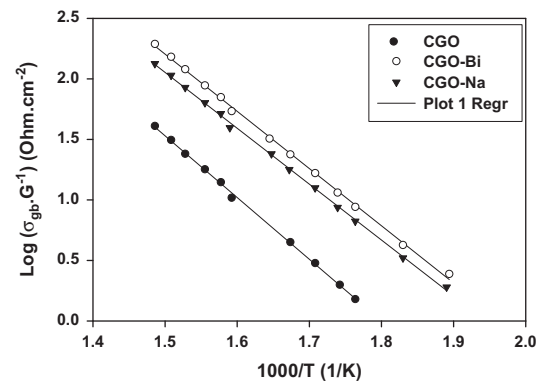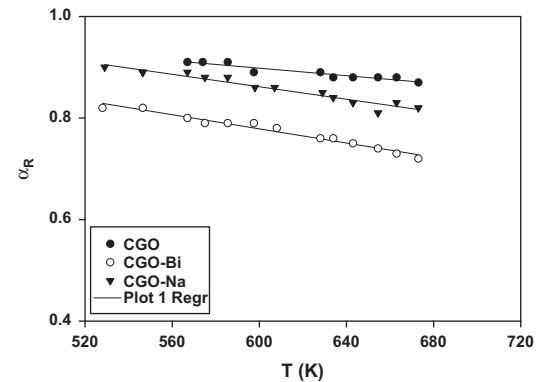

Fig. 5. Temperature dependence of the grain boundary conductivity normalized for the mean grain size.

Fig. 6. Temperature dependence of the blocking factor, α_R. See text for details.

One possible explanation to account for the increase in the grain boundary conductivity and decrease of α_R in CGO-Na is that sodium act as a scavenger for impurities, mainly silicon. The two phenomena, increase of the blocking effect (due to pores and increased grain boundary area) and cleaning of the grain boundaries (scavenger effect), would compete with each other resulting in favor of the latter, and turning the addition of sodium interesting whenever a porous material with high conductivity is required.

4. Conclusions

Microstructural and ionic conductivity results on gadolinia-doped ceria containing small amounts of Bi and Na revealed that these additives results in different microstructures, but similar electrical conductivity effects.

In bismuth-containing samples, densification and grain growth were promoted. For sodium addition, the porosity fraction increased and the mean grain size decreased compared to pure CGO. Both additives enhanced the grain and the grain boundary conductivity of gadolinia-doped ceria, but bismuth addition resulted in a more homogeneous microstructure and higher electrical conductivity.

References

[1] K. Eguchi, Ceramic materials containing rare earth oxides for solid oxide fuel cells, Journal of Alloys and Compounds 250 (1997) 486–491.

[2] B.C.H. Steel, Appraisal of $Ce_{1-y}Gd_yO_{2-y/2}$ electrolytes for IT-SOFC operation at 500 °C, Solid State Ionics 129 (2000) 95–110.

[3] M. Mogensen, N.M. Sammes, G.A. Tompsett, Physical, chemical and electrochemical properties of pure and doped ceria, Solid State Ionics 129 (2000) 63–94.

[4] O. Yamamoto, Solid oxide fuel cells: fundamental aspects and prospects, Electrochimica Acta 45 (2000) 2423–2435.

[5] S. Omar, E.D. Wachsman, J.C. Nino, A co-doping approach towards enhanced ionic conductivity in fluorite-based electrolytes, Solid State Ionics 177 (2006) 3199–3203.

[6] S.K. Tadokoro, E.N.S. Muccillo, Effect of Y and Dy co-doping on electrical conductivity of ceria ceramics, Journal of the European Ceramic Society 27 (2007) 4261–4264.

[7] X.L. Zhao, J.J. Lin, T. Xiao, J.C. Wang, Y.X. Zhang, H.C. Yao, J.S. Wang, Z.J. Li, Effect of Ca co-dopant on the electrical conductivity of Gd-doped ceria, Journal of Electroceramics 28 (2012) 149–157.

[8] D.H. Prasad, S.Y. Park, H. Ji, H.-R. Kim, J.-W. Son, B.-K. Kim, H.-W. Lee, J.-H. Lee, Cobalt oxide co-doping effect on the sinterability and electrical conductivity of nano-crystalline Gd-doped ceria, Ceramics International 38 (2012) S497–S500.

[9] C. Herring, Effect of change of scale on sintering phenomena, Journal of Applied Physics 21 (1950) 301–303.

[10] C. Kleinlogel, L.J. Gauckler, Sintering of nanocrystalline CeO_2 ceramics, Advanced Materials 13 (2001) 1081–1085.

[11] T.S. Zhang, J. Ma, Y.J. Leng, S.H. Chan, P. Hing, J.A. Kilner, Effect of transition metal oxides on densification and electrical properties of Si-containing $Ce_{0.8}Gd_{0.2}O_{2-\delta}$ ceramics, Solid State Ionics 168 (2004) 187–195.

[12] J.D. Nicholas, L.C. De Jonghe, Prediction and evaluation of sintering aids for cerium gadolinium oxide, Solid State Ionics 178 (2007) 1187–1194.

[13] V. Gil, C. Moure, P. Durán, J. Tartaj, Low-temperature densification and grain growth of Bi_2O_3-doped ceria gadolinia ceramics, Solid State Ionics 178 (2007) 359–365.

[14] V. Gil, J. Tartaj, C. Moure, P. Duran, Effect of Bi_2O_3 addition on the sintering and microstructural developement of gadolinia doped ceria ceramics, Journal of the European Ceramic Society 27 (2007) 801–905.

[15] Y.-P. Fu, C.-W. Tseng, P.-C. Peng, Effect of bismuth addition on the electrical conductivity of gadolinium-doped ceria ceramics, Journal of the European Ceramic Society 28 (2008) 85–90.

[16] T.J. Huang, H.F. Li, Direct methane oxidation over a Bi_2O_3–GDC system, Journal of Power Sources 173 (2007) 959–964.

[17] S.K. Tadokoro, E.N.S. Muccillo, Effect of solute dispersion on microstructure and electrical conductivity of $Ce_{0.85}Y_{0.13}Pr_{0.02}O_{2-\delta}$ solid electrolyte, Journal of Power Sources 154 (2006) 1–7.

[18] D.W. Johnson Jr., Nonconventional powder preparation techniques, American Ceramic Society Bulletin 60 (1981) 221–224.

[19] R.D. Shannon, Revised effective ionic radii and systematic studies of interatomic distances in halides and chalcogenides, Acta Crystallographica A32 (1976) 751–767.

[20] R.A. Rocha, E.N.S. Muccillo, Physical and chemical properties of nanosized powders of gadolinia-doped ceria prepared by the cation complexation technique, Materials Research Bulletin 38 (2003) 1979–1986.

[21] J.R. McBride, K.C. Hass, B.D. Poindexter, W.H. Weber, Raman and X-ray studies of $Ce_{1-x}RE_xO_{2-y}$, where RE=La, Pr, Nd, Eu, Gd and Tb, Journal of Applied Physics 76 (1994) 2435–2441.

[22] A.L. Horovistiz, E.N.S. Muccillo, Quantification of microstructural features in gadolinia-doped ceria containing co-additives by digital image analysis, Journal of the European Ceramic Society 31 (2011) 1431–1438.

[23] M. Kleitz, H. Bernard, E. Fernandez, E. Schouler, Impedance spectroscopy and electrical resistance measurements on stabilized zirconia, in: A.H. Heuer, L.W. Hobbs (Eds.), Advances in Ceramics 3, Science and Technology of Zirconia I, American Ceramic Society, Columbus, OH, 1981, pp. 310–336.